Int. J. Electrochem. Sci., 7 **(2012)** 9748 - 9764

International Journal of
ELECTROCHEMICAL
SCIENCE
www.electrochemsci.org

Cyclic Ammonium-Based Ionic Liquids as Potential Electrolytes for Dye-Sensitized Solar Cells

I-Wen Sun[1], *H. Paul Wang*[2], *Hsisheng Teng*[3], *Shyh-Gang Su*[1], *Yuan-Chung Lin*[4], *Chung-Wen Kuo*[5], *Pin-Rong Chen*[6], *Tzi-Yi Wu*[6,*]

[1] Department of Chemistry, National Cheng Kung University, Tainan 70101, Taiwan
[2] Department of Environmental Engineering, National Cheng Kung University, Tainan, Taiwan
[3] Department of Chemical Engineering, National Cheng Kung University, No. 1, University Rd., Tainan, Taiwan 70101, Taiwan
[4] Institute of Environmental Engineering, National Sun Yat-Sen University, Kaohsiung 804, Taiwan
[5] Department of Chemical and Materials Engineering, National Kaohsiung University of Applied Sciences, Kaohsiung 80778, Taiwan
[6] Department of Chemical and Materials Engineering, National Yunlin University of Science and Technology, Yunlin 64002, Taiwan
[*]E-mail: wuty@yuntech.edu.tw

Received: 24 August 2012 / *Accepted:* 19 September 2012 / *Published:* 1 October 2012

Cyclic ammonium-based ionic liquids containing pyrrolidinium, piperidinium, morpholinium-based cations are synthesized, and their thermal properties, viscosities, ion diffusion coefficients, charge transfer resistances, and photovoltaic properties are characterized. A DSSC electrolyte employing Pyr14 (1-butyl-1-methylpyrrolidinium iodide) gives an open circuit voltage of 0.685 V, a short-circuit current of 14.53 mA/cm^2, and conversion efficiency of 6.52 % under light intensity of 100 mW/cm^2 due to Pyr14 possesses the lowest viscosity and highest diffusion coefficient. The DSSC based on Pip14 exhibited 5.55 % conversion efficiency, which is smaller than that of Mor14 (η = 6.19 %) due to an oxygen atom substitutes for a carbon atom.

Keywords: Ionic liquid, cyclic ammonium, electrochemical impedance spectroscopy, Dye-sensitized solar cells.

1. INTRODUCTION

Ionic liquids (ILs) based electrolytes are now well known materials which shows excellent matching with global market demands [1-36]. IL electrolytes are known potential candidate for efficient dye-sensitized solar cell (DSSC) [37-41], the photovoltaic effect in a DSSC originates from

the interface between a redox electrolyte containing iodide and tri-iodide (I^-/I_3^-) ions and a dye-adsorbed mesoscopic TiO_2 electrode [42]. The electrolyte, as one of the key ingredients, provides internal electric conductivity by diffusing within the mesoporous TiO_2 layer [43] and is an important factor in determining the cell performance.

The advancement of dye-sensitized solar cells (DSSCs) with liquid electrolytes from the laboratory level to the industrial level has been impeded by the problems related to the hermetic sealing and evaporation of liquids at high temperatures. Replacing the liquid electrolyte in the DSSC with a quasi-solid electrolyte is expected to solve these technological problems, however, the solar-energy-to-electricity conversion efficiency decreases. In earlier works, the composition of the electrolyte was based on solvents capable to dissolve both iodide salts and iodine, which are the source of the I_3^-/I^- redox couple. Such solvents are, for example, acetonitrile, propylene carbonate, methoxyacetonitrile [44], etc. However, no solvent can be equally good for iodine and iodide salts (for example alkali salts) [45]. In addition, solvent volatility problems and the necessity of costly cell sealing urged for the search of alternative materials. Room temperature ionic liquids (molten salts) have several qualities as compared with other choices since they have negligible volatility and satisfactory ionic conductivity [46]. Ionic liquids are viscous materials, therefore ion diffusion is limited and it is expected to give lower conductivities than common solvents. However, it has been shown that a Grotthus-like mechanism owing to electron exchange between I^- and I_3^- in the redox couple endows ionic liquids with satisfactory conductivity despite the high viscosity value [47].

Accordingly, the objective of this paper is to analyze the influence of the cation component in cyclic ammonium-based ILs on the properties of electrolytes and performance of DSSCs, we studied seven ILs with different cations as DSSCs electrolytes. The thermal properties of these ILs were measured, and electrolytes prepared based on these ILs were characterized by density, viscosity, and electrochemical impedance spectroscopy. Cell performances of the DSSCs assembled based on the prepared ILs-based electrolytes were also characterized. The authors hope that this work will stimulate further discussions and eventually be useful in choosing suitable IL electrolytes to improve the efficiency of DSSCs in the future.

2. EXPERIMENTAL

2.1. Materials and measurement

All starting materials were purchased from Aldrich, Lancaster, TCI, and Acros and used as received. Solvents were freshly distilled prior to use. The ^1H spectra were obtained on a Bruker 400 MHz FT-NMR. Chemical shifts were reported in ppm relative to tetramethylsilane δ units. The density of the electrolyte was measured with a dilatometer, which was calibrated by measuring the density of neat glycerin at 30, 40, 50, 60, 70, and 80 ^oC. The dilatometer was placed in a thermostatic water bath (TV-4000, TAMSON) whose temperature was regulated to within ± 0.01 K. To measure density, the electrolyte was placed into the dilatometer up to the mark, the top of the capillary tube (located on the top of the dilatometer) was sealed, and the dilatometer (with capillary tube) was placed into a

temperature bath for 10 min to allow the temperature to equilibrate. The main interval between the two marks in the capillary tube was 0.01 cm^3, and the minor interval between two marks was 0.001 cm^3. From the correction coefficient of glycerin in capillary tube at various temperatures, we can calculate the density of electrolyte system by the expanded volume of liquid in the capillary tube at various temperatures. Each sample was measured at least three times to determine an average value, and the values of the density were ±0.0001 g mL^{-1}. The viscosities (η) of the electrolytes were measured using a calibrated modified Ostwald viscometer (Cannon-Fenske glass capillary viscometers, CFRU, 9721-A50). The viscometer capillary diameter is 1.2 mm. The measurement of viscometer capillary diameter is implemented by a caliper, model No. PD-153, the accuracy is ± 0.02 mm. The viscometer was placed in a thermostatic water bath (TV-4000, TAMSON), in which the temperature was regulated to within ± 0.01 K. The flow time was measured with a stop watch capable of recording to 0.01 s. For each electrolyte, the experimental viscosity was obtained by averaging three to five flow time measurements. The melting point of each IL was analyzed by using a differential scanning calorimeter (DSC, Perkin–Elmer Pyris 1) in the temperature range -140 ^oC to a predetermined temperature. The sample was sealed in an aluminum pan, and then heated and cooled at scan rate of 10 $^oC\ min^{-1}$ under a flow of nitrogen. The thermal data were collected during heating in the second heating–cooling scan. The thermal stabilities were measured with TGA (Perkin–Elmer, 7 series thermal analysis system). The sample was placed in the platinum pan, and heated at 20 $^oC\ min^{-1}$ from room temperature to 800 ^oC under nitrogen. The water content of the dried ILs was detected by a moisture titrator (Metrohm 73KF coulometer) basing on Karl–Fischer method, and the values were less than 250 ppm. NMR spectra of synthetic ionic liquids were recorded on a BRUKER AV500 spectrometer in D_2O and calibrated with tetramethylsilane (TMS) as the internal reference. Electrochemical impedance spectra of DSSCs were measured in the dark at −0.65V forward bias to determine diffusion coefficients (D_{el}) of triiodide (I_3^-) and charge transfer resistances (R_{CT}) using a Zahner IM6 Impedance Analyzer. The spectra were scanned at room temperature in a frequency range of 0.01 Hz to 100 kHz with the alternated voltage amplitude set at 10 mV.

2.2. Synthetic procedure of cyclic ammonium-based ILs

2.2.1. 1-Butyl-1-methylpyrrolidinium iodide (Pyr14)

To a stirred solution of *N*-methylpyrrolidine (8.51 g, 0.10 mol) in acetonitrile (70 mL) was added requisite aliphatic halide (butyl iodide, 20.24 g, 0.11 mol) dropwise under Ar at 0 ^oC. The reaction mixture was stirred for 24 ~ 48 h at 30 ^oC. Removal of the solvent under reduced pressure, the crude compound was dissolved in 200 mL of water and extracted with dichloromethane at least three times. After removing water on a rotary evaporator, the resulting solid was dried at 100 ^oC under a vacuum for 6 h. In order to eliminate traces of water either coming from the starting materials or from atmosphere, the resulting mixtures were heated at 85 ^oC for 48 h under vacuum of 1 torr. The ionic liquid samples were kept sealed in vials using thick layers of paraffin before uses.

Yield: 91 %. ^1H NMR (400 MHz, D_2O, ppm): 3.45 (m, 4H, N-C$\underline{H}_2$-), 3.28 (t, 2H, N-C$\underline{H}_2$-), 2.99 (s, 3H, N-C$\underline{H}_3$), 2.15 (m, 4H, N-CH_2-C$\underline{H}_2$), 1.73 (m, 2H, N-CH_2-C$\underline{H}_2$), 1.34 (m, 2H, N-CH_2-CH_2-

C$\underline{H}_2$-CH$_3$), 0.90 (t, 3H, N-CH$_2$-CH$_2$-CH$_2$-C$\underline{H}_3$). Elem. Anal. Calcd. for $C_9H_{20}IN$: C, 40.16 %; H, 7.49 %; N, 5.20 %. Found: C, 40.02 %; H, 7.53 %; N, 5.18 %.

Table 1. The denominations and chemical structures of cyclic ammonium-based ILs.

Ionic liquids	Structure
Pyr14	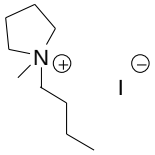
Pip14	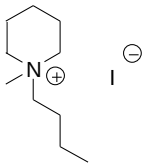
Pip23	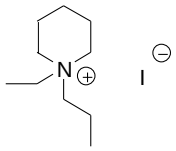
Pip24	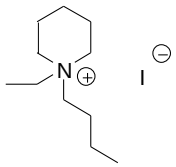
Mor14	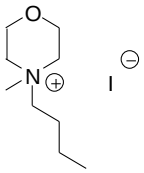
Mor23	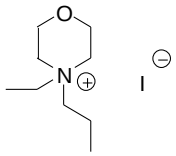
Mor24	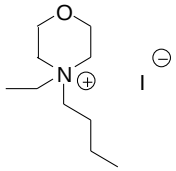

2.2.2. 1-Butyl-1-methylpiperidinium iodide (Pip14)

Yield: 88 %. ^{1}H NMR (400 MHz, D_2O, ppm): 3.39 (m, 4H, N-C$\underline{H}_2$-), 3.25-3.19 (t, 2H, N-C$\underline{H}_2$-), 2.93 (s, 3H, N-C$\underline{H}_3$), 2.10 (m, 4H, N-CH$_2$-C$\underline{H}_2$), 1.86-1.62 (m, 4H, N-CH$_2$-C$\underline{H}_2$ and N-CH$_2$-CH$_2$-C$\underline{H}_2$), 1.32-1.24 (m, 2H, N-CH$_2$-CH$_2$-C$\underline{H}_2$-CH$_3$), 0.86-0.82 (t, 3H, N-CH$_2$-CH$_2$-CH$_2$-C$\underline{H}_3$). Elem. Anal. Calcd. for $C_{10}H_{22}IN$: C, 42.41 %; H, 7.83 %; N, 4.95 %. Found: C, 42.16 %; H, 7.73 %; N, 4.81 %.

2.2.3. 1-Ethyl-1-propylpiperidinium iodide (Pip23)

Yield: 90 %. ^{1}H NMR (400 MHz, D_2O, ppm): 3.35-3.25 (m, 8H, N-C$\underline{H}_2$-), 1.89 (m, 4H, N-CH_2-C$\underline{H}_2$), 1.72 (m, 4H, N-CH_2-C$\underline{H}_2$ and N-CH_2-CH_2-C$\underline{H}_2$), 1.31 (m, 3H, N-CH_2-C$\underline{H}_3$), 1.01 (t, 3H, N-CH_2-CH_2-C$\underline{H}_3$). Elem. Anal. Calcd. for $C_{10}H_{22}$IN: C, 42.41 %; H, 7.83 %; N, 4.95 %. Found: C, 42.22 %; H, 7.79 %; N, 4.85 %.

2.2.4. 1-Butyl-1-ethylpiperidinium iodide (Pip24)

Yield: 94 %. ^{1}H NMR (400 MHz, D_2O, ppm): 3.38-3.22 (m, 8H, N-C$\underline{H}_2$-), 1.85 (m, 4H, N-CH_2-C$\underline{H}_2$), 1.66 (m, 4H, N-CH_2-C$\underline{H}_2$ and N-CH_2-CH_2-C$\underline{H}_2$), 1.39-1.34 (m, 2H, N-CH_2-CH_2-C$\underline{H}_2$-CH_3), 1.26 (t, 3H, N-CH_2-C$\underline{H}_3$), 0.97-0.93 (t, 3H, N-CH_2-CH_2-CH_2-C$\underline{H}_3$). Elem. Anal. Calcd. for $C_{11}H_{24}$IN: C, 44.45 %; H, 8.14 %; N, 4.71 %. Found: C, 44.36 %; H, 8.07 %; N, 4.75 %.

2.2.5. 4-Butyl-4-methylmorpholin-4-ium iodide (Mor14)

Yield: 85 %. ^{1}H NMR (400 MHz, D_2O, ppm): 4.01 (m, 4H, O-C$\underline{H}_2$-), 3.53-3.40 (m, 6H, N-C$\underline{H}_2$-), 3.14 (s, 3H, N-C$\underline{H}_3$), 1.74 (m, 2H, N-CH_2-C$\underline{H}_2$), 1.36 (m, 2H, N-CH_2-CH_2-C$\underline{H}_2$-CH_3), 0.92 (t, 3H, N-CH_2-CH_2-CH_2-C$\underline{H}_3$). Elem. Anal. Calcd. for C_9H_{20}INO: C, 37.91 %; H, 7.07 %; N, 4.91 %. Found: C, 37.79 %; H, 7.07 %; N, 4.85 %.

2.2.6. 4-Ethyl-4-propylmorpholin-4-ium iodide (Mor23)

Yield: 87 %. ^{1}H NMR (400 MHz, D_2O, ppm): 4.05 (m, 4H, O-C$\underline{H}_2$-), 3.51-3.41 (m, 8H, N-C$\underline{H}_2$-), 1.77 (m, 2H, N-CH_2-C$\underline{H}_2$), 1.34 (t, 3H, N-CH_2-C$\underline{H}_3$), 1.01 (t, 3H, N-CH_2-CH_2-C$\underline{H}_3$). Elem. Anal. Calcd. for C_9H_{20}INO: C, 37.91 %; H, 7.07 %; N, 4.91 %. Found: C, 37.81 %; H, 7.01 %; N, 4.82 %.

2.2.7. 4-Butyl-4-ethylmorpholin-4-ium iodide (Mor24)

Yield: 90 %. ^{1}H NMR (400 MHz, D_2O, ppm): 4.03 (m, 4H, O-C$\underline{H}_2$-), 3.54-3.38 (m, 8H, N-C$\underline{H}_2$-), 1.69 (m, 2H, N-CH_2-C$\underline{H}_2$), 1.41-1.30 (m, 5H, N-CH_2-CH_2-C$\underline{H}_2$-CH_3 and N-CH_2-C$\underline{H}_3$), 0.97-0.94 (t, 3H, N-CH_2-CH_2-CH_2-C$\underline{H}_3$). Elem. Anal. Calcd. for $C_{10}H_{22}$INO: C, 40.14 %; H, 7.41 %; N, 4.68 %. Found: C, 40.03 %; H, 7.36 %; N, 4.65 %.

2.3. Preparation of dye-sensitized TiO_2 electrode (photoanode) and counter electrode

F-doped tin oxide (FTO) glass plates (3 mm thickness, 7 Ω cm^{-2}) were first cleaned ultrasonically in a cleaning detergent solution for 15 min, and rinsed with water and ethanol. The FTO electrodes were then immersed into 40 mM $TiCl_4$ (aqueous) at 70 ^oC for 30 min and rinsed with water

and ethanol. Two kinds of TiO_2 paste, containing nanocrystalline (~25 nm) TiO_2 (Degussa P25, paste A) and submicroparticle TiO_2 (500 nm, paste B), respectively, were prepared using a previously reported procedure [44]. To prepare paste A, commercial titania powder (3 g, Degussa P25) was ground in a mortar with a small amount of water (1 mL) containing acetylacetone (0.1 mL). After the TiO_2 particles were dispersed, the paste was diluted with 3 mL water under continued grinding and a surfactant, Triton X-100 (0.05 mL), was added to facilitate the spreading of the colloid on the substrate. Paste A was sonicated for about 24 h at 28 ^oC. TiO_2 film (12 μm) was prepared by spin coating. After paste A was dried at 125 ^oC, ~4 μm thick paste B was spin-coated on top of it. The electrodes coated with TiO_2 pastes were gradually heated (5 $^oC\ min^{-1}$) under airflow up to 450 ^oC for 30 min followed by treating with 40 mM $TiCl_4$, rinsed with water and ethanol, and sintered again at 450 ^oC for 30 min. The electrodes with an active area of 0.5 cm × 0.5 cm were immersed in a 1:1 acetonitrile and isoporpanol solution containing 3×10^{-4} M of dye. The dye-adsorbed TiO_2 films were then rinsed with dry ethanol, and dried in air. A counter electrode was prepared by sputtering a thin platinum layer (50 nm) on an FTO substrate. The thicknesses of the TiO_2 films were determined by profilometry. Platinum sputtering was carried out using a Hitachi E 1045 instrument. The platinum layer thickness on the glass substrates was estimated using the amount of sputtered platinum recorded on a quartz thickness monitor.

2.4. DSSC assembly

The dye adsorbed TiO_2 electrode and Pt-counter electrode were assembled into a sandwich sealed type cell by heating them with hot-melt ionomer film (60 μm thickness, Solaronix) as a spacer. A drop of electrolyte solution (0.1 M LiI, 0.05 M I_2, 0.6 M DMPII and 0.5 M tert-butyl pyridine (TBP) in acetonitile (ACN)) was injected through a hole in the counter electrode, which was then sealed with hot-melt ionomer film and glass. The electrolyte was introduced into the cell and sealed with AB epoxy for 30 min. The working area of the electrode was 0.25 cm^2.

2.5. Photovoltaic measurements of the solar cells

The photovoltaic measurements of the DSSCs were performed using a Newport M-66907 450 W xenon light source through an infrared blocking filter and a Keithley 2400 digital source meter linked to a computerized control and data acquisition system. The light intensity was 1000 $W \cdot m^{-2}$ under an AM 1.5 light source. Cell temperatures were kept at 25 ^oC during the illumination. Light intensity was calibrated using a mono-Si reference solar cell (PVM134). A 300W xenon arc lamp solar simulator (#91160A, Oriel) with an AM 1.5 Globe filter (#59044, Oriel) was used to measure the I-V characteristics of the quasi-solid-state DSSC. The illumination was fixed at 100 $mW \cdot cm^{-2}$ using a reference solar cell and meter (#91150, Oriel).

3. RESULTS AND DISCUSSION

3.1. Thermal Property

The structures of the cyclic ammonium-based ionic liquids prepared and studied in the present work are shown in Table 1. Thermal stability of the synthesized cyclic ammonium-based ionic liquids is studied using TGA and the decomposition temperatures of 10% weight loss are summarized in Table 2. Each ionic liquid used for thermal property measurements was dried under vacuum at 393 K for 24 h before use. Figure 1 shows the thermogravimetric traces of these ILs. The thermal decomposition temperatures (T_d) of these ILs has some relationship with the structure of cations, the thermal stability of these cations follows the order: piperidinium (Pip14: 261 ^oC) > pyrrolidinium (Pyr14: 256 ^oC) > morpholinium (Mor14: 241 ^oC). For piperidinium and morpholinium based ionic liquids, Pip23 exhibits higher T_d (292 ^oC) than that of Pip14 and Pip24 (261 and 260 ^oC, respectively), Mor23 exhibits higher T_d (272 ^oC) than that of Mor14 and Mor24 (241 and 238 ^oC, respectively), implying symmetrical alkyl substitute in the cations increases the thermal stability significantly. The good thermal stability of the synthesized cyclic ammonium-based ionic liquids (T_d > 238 ^oC) enables their potential use for electrolytes in Dye-sensitized solar cell.

Table 2. Thermal properties of cyclic ammonium-based ionic liquids

Ionic liquid	M_w / g mol^{-1}	T_g / $^\circ$C	T_{s-s} / $^\circ$C	T_m / $^\circ$C	T_d / $^\circ$C
Pyr14	269.17	-91	-24, 8	153	256
Pip14	283.19	-25	53	184	261
Pip23	283.19	-42	---	67	292
Pip24	297.22	---	77	128	260
Mor14	285.17	-16	---	125	241
Mor23	285.17	---	---	87	272
Mor24	299.19	-40	---	103	238

[a] Decomposition temperature (T_d) of 10 % weight loss.

The phase transitions temperature is an important issue to evaluate the liquid or gel state of ionic liquid electrolyte. Thermal properties of the ionic liquid electrolytes were investigated by differential scanning calorimetry. The phase transitions were observed on a second heating, the melting point (T_m) and glass transition point (T_g) were summarized in Table 2. By inspecting the transition temperatures as a function of the cation, it can be noted that the glass transition temperature (T_g) of the pyrrolidinium-based IL (Pyr14: T_g = -91 ^oC) is lower than piperidinium-based IL (Pip14: T_g = -25 ^oC) and morpholinium-based IL (Mor14: T_g = -16 ^oC).

The typical DSC thermograms are reported in Figure 2. One type of behavior characterized by ILs exhibits a melting transition, such as morpholinium based ILs (Mor23). A second form of behavior arises from samples such as Pip24 with a solid-solid transition (T_{s-s} = 77) before T_m were observed. The third type of behavior was from sample Pyr14 with multiple solid-solid transitions (T_{s-s} = -24, 8 ^oC) before T_m and with substantial supercooling as the freezing points (T_c = -51 ^oC) of the samples are significantly lower than the corresponding melting points.

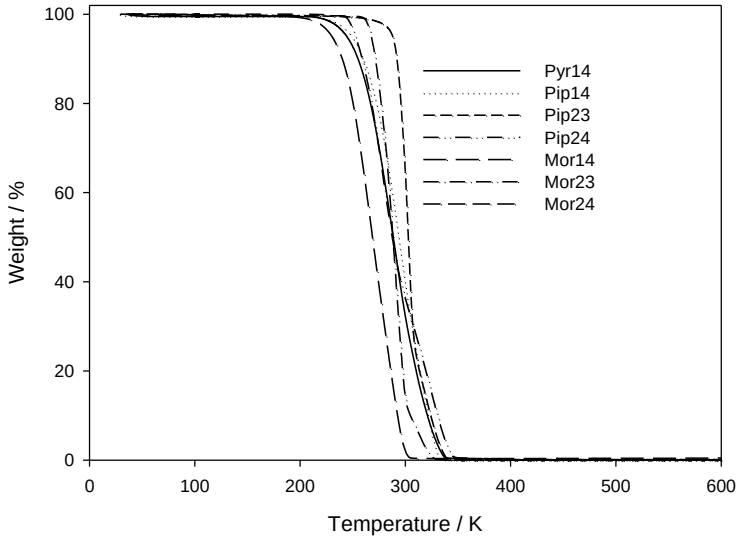

Figure 1. Thermogravimetric trace for these cyclic ammonium-based ionic liquids under nitrogen atmospheres.

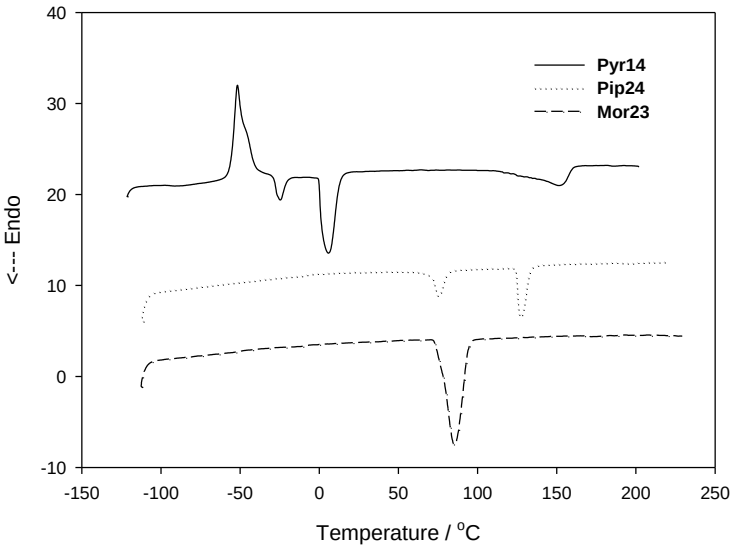

Figure 2. Selected DSC thermogram of ILs obtained from DSC heating experiment.

3.2. The temperature dependence of the density and viscosity of IL-based electrolytes

Viscosity measurement is an important issue to estimate the ionic conductivity of electrolyte due to ionic transport. In general, viscosities at room temperature are enough for solar cell application. For outdoor use, viscosities at higher temperatures become important parameters. The temperature-dependent densities (ρ) were characterized to evaluate the kinematic viscosity and were fitted to a linear equation as shown in Eqn. 1 by using linear regression techniques

$$\rho = A + BT \qquad (1)$$

where A and B are constants and T is the absolute temperature. The adjustable parameters of Eqn. 1 for density of these ILs-based electrolytes are summarized in Table 4.

Table 3. Temperature dependence of density and dynamic viscosity (η) data for DSSC electrolyte (0.1 M LiI, 0.05 M I_2, 0.6 M cyclic ammonium-based ionic liquids (Pyr14, Pip14, Pip23, Pip24, Mor14, Mor23, Mor24), 0.5 M tert-butyl pyridine (TBP) in acetonitile (ACN)).

Pyr14			***Pip14***			***Pip23***			***Pip24***		
T (K)	ρ (g/cm^3)	η (cp)	T (K)	ρ (g/cm^3)	η (cp)	T (K)	ρ (g/cm^3)	η (cp)	T (K)	ρ (g/cm^3)	η (cp)
305	0.857	0.548	304.5	0.862	0.572	303.0	0.864	0.563	303.8	0.873	0.574
308	0.854	0.537	307.0	0.860	0.546	306.0	0.862	0.549	307.2	0.871	0.554
311.2	0.851	0.522	308.8	0.858	0.532	308.8	0.859	0.534	310.5	0.868	0.539
314.1	0.849	0.510	311.0	0.856	0.523	312.2	0.856	0.520	313.5	0.865	0.527
317.1	0.846	0.498	314.0	0.854	0.512	315.1	0.853	0.510	316.1	0.863	0.516
320	0.843	0.487	317.0	0.851	0.501	318.0	0.851	0.498	320.0	0.859	0.505
323.5	0.840	0.475	320.0	0.848	0.490	321.0	0.848	0.488	323.0	0.857	0.499
326	0.837	0.469	323.3	0.845	0.479	325.0	0.844	0.475	325.8	0.854	0.492
328.8	0.835	0.459	327.0	0.841	0.467	327.0	0.842	0.468	328.8	0.852	0.488
332	0.831	0.448	330.0	0.839	0.458	329.8	0.839	0.460	331.0	0.849	0.480
335	0.828	0.440	333.0	0.835	0.449	332.2	0.836	0.452			

Mor14			***Mor23***			***Mor24***		
T (K)	ρ (g/cm^3)	η (cp)	T (K)	ρ (g/cm^3)	η (cp)	T (K)	ρ (g/cm^3)	η (cp)
302.8	0.858	0.574	305.0	0.858	0.573	304.0	0.858	0.572
307.0	0.855	0.553	308.5	0.857	0.542	307.0	0.856	0.557
309.8	0.853	0.539	311.0	0.854	0.533	309.5	0.853	0.547
312.0	0.850	0.531	314.3	0.851	0.517	313.0	0.850	0.530
315.0	0.848	0.519	317.5	0.848	0.504	316.0	0.847	0.515
318.0	0.845	0.507	320.5	0.845	0.495	319.0	0.846	0.508
321.0	0.842	0.495	323.8	0.842	0.481	322.0	0.843	0.496
324.0	0.839	0.484	328.0	0.838	0.466	325.0	0.840	0.485
327.0	0.836	0.474	332.0	0.834	0.454	327.8	0.837	0.474
329.5	0.833	0.465	334.0	0.831	0.448	330.2	0.835	0.465
332.5	0.830	0.457				333.2	0.832	0.456

The kinematic viscosity data obtained with the modified Oswald viscometer were converted to dynamic or absolute viscosities, η, by using the following equation

$$\text{Kinematic viscosity} = \eta/\rho \qquad (2)$$

An Arrhenius plot of ln η vs $1/T$ was constructed from the experimental data and a linear relationship was found. A linear equation of the form was fitted to the experimental data.

$$\ln \eta = A + B(10^3 \times 1/T) \qquad (3)$$

The fitted values of A and B are collected in Table 4. However, some observed temperature dependence of viscosity are not linear but polynomial (n = 2 or n = 3), and are often best fitted by the Fulcher equation (or more commonly called VTF equation) [48-57].

$$\eta = \eta_o \exp[\frac{B}{(T - T_o)}] \quad (4)$$

where T is the absolute temperature, and η_o, B, and T_o are adjustable parameters. The best-fit η_o (cP), B (K), and T_o (K) parameters are given in Table 5. The electrolyte (0.1 M LiI, 0.05 M I_2, 0.6 M cyclic ammonium-based ionic liquids, 0.5 M tert-butyl pyridine (TBP) in acetonitile (ACN), total 12 ml) exhibits a low absolute viscosity (ca 0.54 ~ 0.58 cp at 30 ^oC). Based on the concern of higher mass transport, it is expected that these IL-based electrolytes should be an appropriate media for the electrolyte of dye-sensitized solar cell.

Table 4. Fitted parameters of DSSC electrolyte for $\rho = A + BT$, ρ, density (g/cm^3), and for ln $\eta = A + B(10^3 \times 1/T)$, η, absolute viscosity (cp).

	Ionic liquids	A	B	R^2
Density	Pyr14	1.1492	-9.5723×10^{-4}	0.9996
	Pip14	1.1448	-9.2854×10^{-4}	0.9989
	Pip23	1.15	-9.421×10^{-4}	0.9988
	Pip24	1.144	-8.883×10^{-4}	0.9990
	Mor14	1.1476	-9.5348×10^{-4}	0.9985
	Mor23	1.1484	-9.469×10^{-4}	0.9968
	Mor24	1.13	-8.936×10^{-4}	0.9976
Viscosity	Pyr14	-3.0768	0.7552	0.9993
	Pip14	-3.193	0.7946	0.9841
	Pip23	-3.0503	0.7492	0.9992
	Pip24	-2.6456	0.6306	0.9809
	Mor14	-3.1119	0.7735	0.9996
	Mor23	-3.2741	0.8237	0.9918
	Mor24	-3.1378	0.7839	0.9987

Table 5. VTF equation parameters of viscosity for some DSSC electrolytes. ($\eta = \eta_o \exp[-B/(T - T_o)]$).

Ionic liquids	η_o (cp)	T_o (K)	B (K)[a]	R^{2b}
Pip14	0.3246	262.7	23.3	0.993
Pip24	0.3824	268.0	14.5	0.999
Mor23	0.261	238.6	51.8	0.996

[a] Activation energy (kJ mol^{-1}).

[b] Correlation coefficient.

3.3. Electrochemical properties

Electrochemical impedance spectroscopy (EIS) is a powerful technique for the characterization of electronic or ionic transport processes in DSSCs [58]. Figure 3(a) shows the impedance spectra of

the dye-sensitized TiO_2 solar cell prepared with liquid electrolyte ((0.1 M LiI, 0.05 M I_2, 0.6 M cyclic ammonium-based ionic liquids (Pyr14, Pip14, Pip23, Pip24, Mor14, Mor23, Mor24), 0.5 M tert-butyl pyridine (TBP) in acetonitile (ACN)), and an equivalent circuit corresponding to the DSSCs is shown in Figure 3(b). The measurements are carried out at the open-circuit voltage and under 100 mW cm^{-2} illumination. The parameters listed in Table 6 are obtained by fitting the spectra with the equivalent circuit, different impedance elements are contributing to the impedance spectrum of a thin layer cell. Most of the spectra exhibit three semicircles, which were assigned, from left to right, to the electrochemical reaction at the Pt counter electrode (Z_1), the reaction at the TiO_2/dye/electrolyte interface (Z_2) and the diffusion of I_3^- at the Pt/electrolyte interface (Z_3) [59]. The values of R_{CT1}, R_{CT2} and R_3 are described as the real parts of Z_1, Z_2, and Z_3, respectively, and were always used to evaluate the internal resistances involved in the corresponding reactions. For high frequencies, the serial resistance (R_S) is dominating the impedance of the cell. In the frequency range between 100 Hz and 10 kHz, the impedance is dominated by the RC network of the Pt/electrolyte interface, consisting of the charge-transfer resistance (R_{CT}) and the capacitance (C) of the electrical double layer. In the range of 1~10 Hz, the Nernst diffusion impedance (Z_N) is visible.

(a)

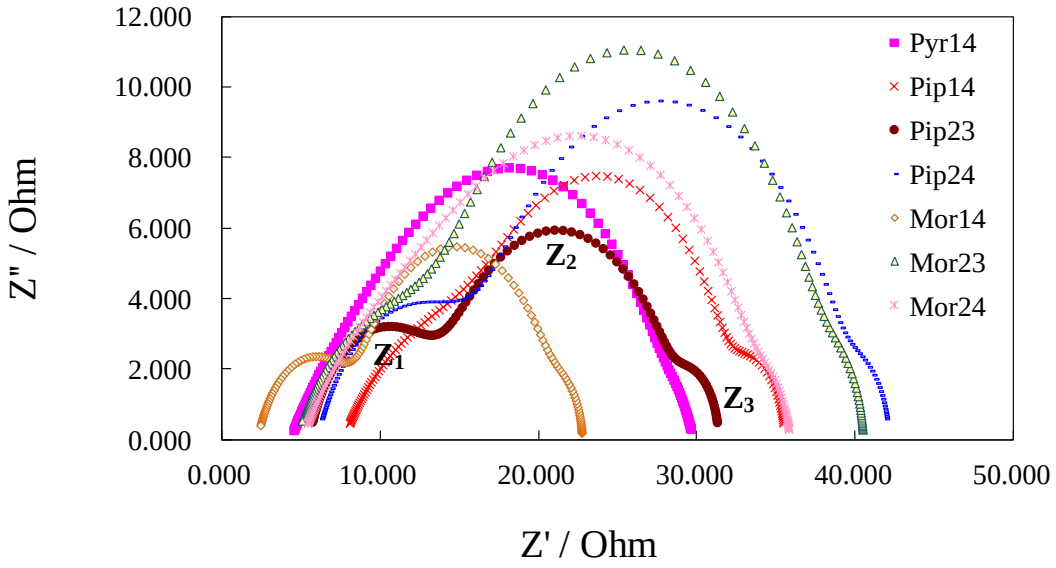

(b)

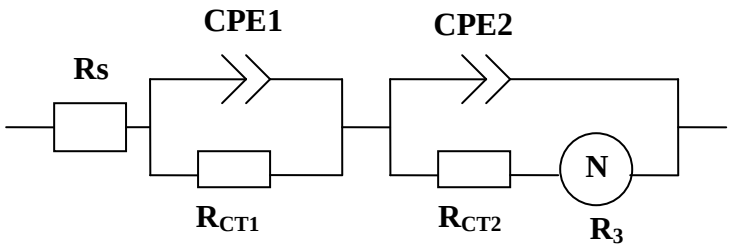

Figure 3. (a) Nyquist diagrams of the impedance spectra obtained for a dye-sensitized TiO_2 solar cell prepared with liquid electrolyte ((0.1 M LiI, 0.05 M I_2, 0.6 M cyclic ammonium-based ionic liquids (Pyr14, Pip14, Pip23, Pip24, Mor14, Mor23, Mor24), 0.5 M tert-butyl pyridine (TBP) in acetonitile (ACN)). (b) Equivalent circuit of DSSC for fitting model.

Table 6. Characteristic fitting parameters of equivalent circuit; series resistances (R_s/W) and charge transfer resistances (R_{CT}/W), constant phase element (CPE/μF), Warburg parameter (W/Ω $s^{-1/2}$) and triiodide diffusion coefficients (D_{el}/cm^2 s^{-1}) of IL electrolytes.

Ionic liquids	Pyr14	Pip14	Pip23	Pip24	Mor14	Mor23	Mor24
R_s (Ω)	4.276	7.624	5.431	5.846	2.2	4.644	4.991
R_{CT1} (Ω)	13.81	12.36	8.696	10.85	6.468	11.2	12.98
CPE1 (μF)	35.67	19.14	9.101	9.061	11.34	13.03	20.4
R_{CT2} (Ω)	10.79	11.92	14.05	22.35	11.85	21.59	16.15
CPE2 (μF)	269.9	373.6	235.5	189.8	322.9	184.9	130.3
W (Ω $s^{-1/2}$)	2.005	6.012	4.247	3.755	4.46	6.414	3.697
k (1/s)	4.589	2.637	1.791	1.61	4.085	4.327	4.19
D_{el} (cm^2/s)	4.13×10^{-5}	2.37×10^{-5}	1.61×10^{-5}	1.45×10^{-5}	3.68×10^{-5}	3.89×10^{-5}	3.77×10^{-5}

The diffusion coefficient of triiodide is one of the most important variables for the optimisation of electrolytes applied in Grätzel-type dye-sensitised solar cells (DSSCs) [60]. For application in dye-sensitised solar cells a preferably high triiodide diffusion coefficient in the electrolyte is required. When the diffusing species is present in an electrolyte, D_{el} is just the diffusion coefficient of this species. Therefore in mixtures containing the I^-/I_3^- redox couple with an excess amount of iodide, D_{el} is given by the diffusion coefficient of triiodide, $D_{I_3^-}$. The diffusion of the tri-iodide in the electrolyte is described by a Nernst impedance Z_N [61],

$$Z_N = \frac{W}{\sqrt{i\omega}} \tanh\left(\sqrt{\frac{\sqrt{i\omega}}{K_N}}\right) \quad (5)$$

where W is the Warburg parameter, and K_N is the time constant. W and K_N are described by following Eqns.

$$W = \frac{kT}{m^2 e_0^2 c_{I_3^-} - A\sqrt{D_{el}}} \quad (6)$$

$$K_N = \frac{D_{el}}{\delta^2} \quad (7)$$

where D_{el} is the diffusion constant of I_3^-, $c_{I_3^-}$ is the concentration of I_3^-, A is the electrode area, m is number of electrons transferred in each reaction (m = 2 for the present discussion, k is Boltzman constant, T is temperature, e_0 is elementary charge; δ is the thickness of the Nernst diffusion layer (δ = 0.5d_{el}; d_{el}, distance between the electrodes: 60 μm).

The diffusion constant D_{el} of the DSSCs was determined by fitting the impedance values and was given in Table 6. The diffusion constant of I_3^- for the ionic liquids was found in the order: (1)

$(D_{el})_{Pyr14} > (D_{el})_{Mor14} > (D_{el})_{Pip14}$; (2) $(D_{el})_{Pip14} > (D_{el})_{Pip23} > (D_{el})_{Pip24}$. The higher D_{el} value gives the larger photocurrent due to the quick charge transport in the electrolyte.

3.4. Photovoltaic performances

DSSCs were prepared and compared to investigate the relationships between the electrolyte behavior of pyrrolidinium, piperidinium, and morpholinium-based ILs and their structures. Typical photocurrent–photovoltage (*I–V*) curves for DSSC cells based on these electrolytes (0.1 M LiI, 0.05 M I_2, 0.6 M cyclic ammonium-based ionic liquids (Pyr14, Pip14, Pip23, Pip24, Mor14, Mor23, Mor24), 0.5 M tert-butyl pyridine (TBP) in acetonitile (ACN)) are shown in Fig. 4. The detailed photovoltaic parameters are summarized in Table 7.

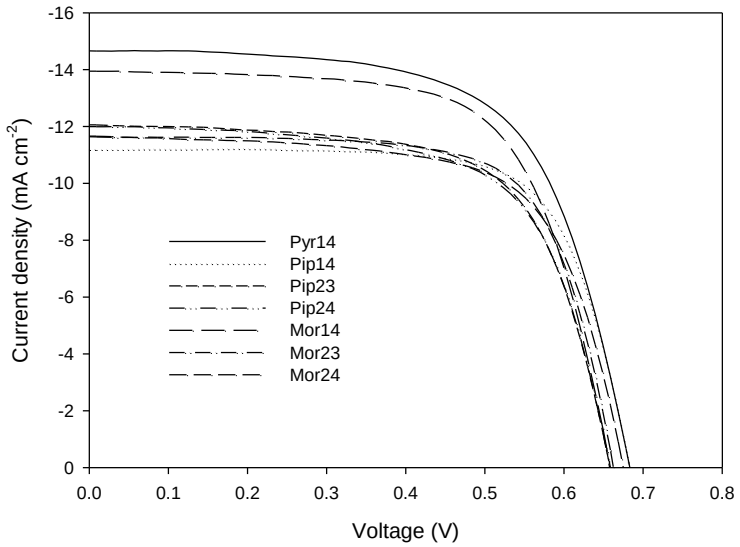

Figure 4. Current density-voltage characteristics for dye-sensitized solar cell assembled with cyclic ammonium-based ionic liquids electrolyte under illumination of simulated solar light (AM 1.5, 100 mW/cm^2).

Table 7. Photovoltaic performances of the DSSCs under 100 mW cm^{-2} light intensity and AM1.5 global radiation.

Ionic liquids	Pyr14	Pip14	Pip23	Pip24	Mor14	Mor23	Mor24
V_{oc}/mV	685	685	661	661	661	663	679
J_{sc}/mA cm^{-2}	14.53	11.16	12.14	11.95	13.97	11.63	11.69
Fill factor (ff)	0.66	0.73	0.66	0.66	0.67	0.72	0.67
η (%)	6.52	5.55	5.33	5.24	6.19	5.52	5.34
V_{mpp}/V	0.517	0.56	0.517	0.522	0.506	0.533	0.533
I_{mpp}/mA cm^{-2}	10.16	10.29	9.714	10.03	12.22	7.948	10.02
MPP/mW	5.252	5.763	5.024	5.242	6.188	4.239	5.34

The photoelectronic performance [i.e. fill factor (FF) and overall conversion efficiency (η)] were calculated by the following equations [62]:

$$\mathrm{FF} = \frac{V_{\max} \cdot J_{\max}}{V_{oc} \cdot J_{sc}} \tag{8}$$

$$\eta(\%) = \frac{V_{\max} \cdot \mathrm{I}_{\max}}{P_{in}} \frac{V_{oc} \cdot J_{sc} \cdot \mathrm{FF}}{P_{in}} \tag{9}$$

where J_{sc} is the short-circuit current density (mA cm^{-2}), V_{oc} is the open-circuit voltage (V), P_{in} is the incident light power (mW cm^{-2}), and J_{max} (mA cm^{-2}) and V_{max} (V) are the current density and voltage in the *I–V* curves, respectively, at the point of maximum power output.

Under the standard global AM 1.5 solar condition, the DSSCs with the electrolyte composed of 0.1 M LiI, 0.05 M I_2, 0.6 M cyclic ammonium-based ionic liquids Pyr14, 0.5 M tert-butyl pyridine (TBP) in acetonitile (ACN), gave short circuit photocurrent density of 14.53 mA cm^{-2}, open circuit voltage of 0.685 V, and fill factor of 0.66, corresponding to the photoelectric conversion efficiency of 6.52 % at the illumination (100 mW cm^{-2}). Under similar conditions, the photoelectric conversion efficiency of cells with the piperidinium-based electrolyte Pip14, Pip23, and Pip24 are 5.55, 5.33, and 5.24 %, respectively, and those of the morpholinium-based electrolyte Mor14, Mor23, and Mor24 are 6.19, 5.52, and 5.34 %, respectively. As seen from Table 3, The Pyr14-based electrolyte has the lowest viscosity value, this suggests that the DSSC for Pyr14 should have the highest short circuit current and highest efficiency. In fact, it is seen that the Pyr14-based electrolyte gives the highest I_{sc} and η values among the investigated DSSCs. For piperidinium- and morpholinium-based electrolyte, increasing the side chain length of cation from methyl (Mor14) to ethyl (Mor24), respectively, slightly decreases efficiency from 6.19 % to 5.34%; and from propyl (Mor23) to butyl (Mor24), respectively, slightly decreases efficiency from 5.52% to 5.34% because of larger cation size has lower diffusion coefficient [63].

As seen in Table 6 and Table 7, the DSSC cell for Pyr14 has the highest current of 14.53 mA cm^{-2}, demonstrating that the larger diffusion coefficient for the DSSCs, in general cause the great short circuit current. Moreover, charge transfer resistance is related with charge recombination reactions in the TiO_2/dye/electrolyte interface (R_{CT2}). Among theses DSSCs, the DSSC cell for Pyr14 has the lowest R_{CT2} value, implying Pyr14 shows the lowest charge losses in the TiO_2/electrolyte interface.

4. CONCLUSIONS

Several low cost ILs containing pyrrolidinium, piperidinium, and morpholinium units as cation were synthesized. These ionic liquid electrolytes were characterized by thermogravimetric trace, DSC heating experiment, density, viscosity, charge transfer resistance, diffusion coefficient measurements, and applied these ILs in DSSCs as electrolyte and investigated photovoltaic performances. The DSSCs with the Pyr14-based electrolyte, which was composed of 0.1 M LiI, 0.05 M I_2, 0.6 M cyclic

ammonium-based ionic liquids Pyr14, and 0.5 M tert-butyl pyridine (TBP) in acetonitile (ACN), gave short circuit photocurrent density of 14.53 mA cm^{-2}, open circuit voltage of 0.685 V, and fill factor of 0.66, corresponding to the photoelectric conversion efficiency of 6.52% at the illumination (Air Mass 1.5, 100 mW cm^{-2}).

ACKNOWLEDGEMENTS
The authors would like to thank the National Science Council of the Republic of China for financially supporting this project. We are very grateful to Ms. Ru-Rong Wu for her help in performing the NMR experiments.

References

1. R.D. Rogers, *Nature*, 447 (2007) 917.
2. M.R. Ganjali, H. Ganjali, M. Hosseini, P. Norouzi, *Int. J. Electrochem. Sci.,* 5 (2010) 967.
3. V.S.R. Channu, R. Holze, E.H. Walker, S.A. Wicker, R.R. Kalluru, Q.L. Williams, W. Walters, *Int. J. Electrochem. Sci.,* 5 (2010) 1355.
4. T.Y. Wu, S.G. Su, K.F. Lin, Y.C. Lin, H.P. Wang, M.W. Lin, S.T. Gung, I.W. Sun, *Electrochim. Acta*, 56 (2011) 7278.
5. M.R. Ganjali, S. Aghabalazadeh, M. Rezapour, M. Hosseini, P. Norouzi, *Int. J. Electrochem. Sci.,* 5 (2010) 1743.
6. M.T. Montañés, R. Sánchez-Tovar, J. García-Antón, V. Pérez-Herranz, *Int. J. Electrochem. Sci.,* 5 (2010) 1934.
7. T.Y. Wu, B.K. Chen, L. Hao, C.W. Kuo, I.W. Sun, *J. Taiwan Inst. Chem. Eng.,* 43 (2012) 313.
8. M. Pandurangachar, B.E.K. Swamy, B.N. Chandrashekar, O. Gilbert, S. Reddy, B.S. Sherigara, *Int. J. Electrochem. Sci.,* 5 (2010) 1187.
9. M.R. Ganjali, M. Rezapour, S.K. Torkestani, H. Rashedi, P. Norouzi, *Int. J. Electrochem. Sci.,* 6 (2011) 2323.
10. T.Y. Wu, B.K. Chen, L. Hao, Y.C. Peng, I.W. Sun, *Int. J. Mol. Sci.,* 12 (2011) 2598.
11. P. Norouzi, Z. Rafiei-Sarmazdeh, F. Faridbod, M. Adibi, M.R. Ganjali, *Int. J. Electrochem. Sci.,* 5 (2010) 367.
12. M.R. Ganjali, M. Hosseini, M. Pirali-Hamedani, H.A. Zamani, *Int. J. Electrochem. Sci.,* 6 (2011) 2808.
13. T.Y. Wu, I.W. Sun, S.T. Gung, B.K. Chen, H.P. Wang, S.G. Su, *J. Taiwan Inst. Chem. Eng.,* 42 (2011) 874.
14. F. Faridbod, M.R. Ganjali, M. Pirali-Hamedani, P. Norouzi, *Int. J. Electrochem. Sci.,* 5 (2010) 1103.
15. M.R. Ganjali, T. Poursaberi, M. Khoobi, A. Shafiee, M. Adibi, M. Pirali-Hamedani, P. Norouzi, *Int. J. Electrochem. Sci.,* 6 (2011) 717.
16. T.Y. Wu, S.G. Su, H.P. Wang, Y.C. Lin, S.T. Gung, M.W. Lin, I.W. Sun, *Electrochim. Acta,* 56 (2011) 3209.
17. P. Norouzi, M. Hosseini, M.R. Ganjali, M. Rezapour, M. Adibi, *Int. J. Electrochem. Sci.,* 6 (2011) 2012.
18. M.R. Ganjali, M.H. Eshraghi, S. Ghadimi, S.M. Moosavi, M. Hosseini, H. Haji-Hashemi, P. Norouzi, *Int. J. Electrochem. Sci.,* 6 (2011) 739.
19. T.Y. Wu, I.W. Sun, S.T. Gung, B.K. Chen, H.P. Wang, S.G. Su, *J. Taiwan Inst. Chem. Eng.,* 43 (2012) 58.

20. M.R. Ganjali, M.R. Moghaddam, M. Hosseini, P. Norouzi, *Int. J. Electrochem. Sci.,* 6 (2011) 1981.
21. H.A. Barham, S.A. Brahim, Y. Rozita, K.A. Mohamed, *Int. J. Electrochem. Sci.,* 6 (2011) 181.
22. P.N. Tshibangu, S.N. Ndwandwe, E.D. Dikio, *Int. J. Electrochem. Sci.,* 6 (2011) 2201.
23. T.H. Tsai, K.C. Lin, S.M. Chen, *Int. J. Electrochem. Sci.,* 6 (2011) 2672.
24. Y.X. An, P.J. Zuo, X.Q. Cheng, L.X. Liao, G.P. Yin, *Int. J. Electrochem. Sci.,* 6 (2011) 2398.
25. P. Norouzi, M. Pirali-Hamedani, S.O. Ranaei-Siadat, M.R. Ganjali, *Int. J. Electrochem. Sci.,* 6 (2011) 3704.
26. F. Faridbod, H.A. Zamani, M. Hosseini, M. Pirali-Hamedani, M.R. Ganjali, P. Norouzi, *Int. J. Electrochem. Sci.,* 6 (2011) 3694.
27. M.R. Ganjali, S.O. Ranaei-Siadat, H. Rashedi, M. Rezapour, P. Norouzi, *Int. J. Electrochem. Sci.,* 6 (2011) 3684.
28. S.K. Shukla, L.C. Murulana, E.E. Ebenso, *Int. J. Electrochem. Sci.,* 6 (2011) 4286.
29. H. Wang, L.X. Wu, Y.C. Lan, J.Q. Zhao, J.X. Lu, *Int. J. Electrochem. Sci.,* 6 (2011) 4218.
30. N.V. Likhanova, O. Olivares-Xometl, D. Guzman-Lucero, M.A. Dominguez-Aguilar, N. Nava, M. Corrales-Luna, M.C. Mendoza, *Int. J. Electrochem. Sci.,* 6 (2011) 4514.
31. S. Ibrahim, M.R. Johan, *Int. J. Electrochem. Sci.,* 6 (2011) 5565.
32. M.R. Ganjali, T. Alizadeh, F. Azimi, B. Larjani, F. Faridbod, P. Norouzi, *Int. J. Electrochem. Sci.,* 6 (2011) 5200.
33. L.C. Xuan, Y.X. An, W. Fang, L.X. Liao, Y.L. Ma, Z.Y. Ren, G.P. Yin, *Int. J. Electrochem. Sci.,* 6 (2011) 6590.
34. B. Baek, S. Lee, C. Jung, *Int. J. Electrochem. Sci.,* 6 (2011) 6220.
35. J. Gao, J.G. Liu, W.M. Liu, B. Li, Y.C. Xin, Y. Yin, Z.G. Zou, *Int. J. Electrochem. Sci.,* 6 (2011) 6115.
36. H. Ganjali, M.R. Ganjali, T. Alizadeh, F. Faridbod, P. Norouzi, *Int. J. Electrochem. Sci.,* 6 (2011) 6085.
37. T.Y. Wu, M.H. Tsao, F.L. Chen, S.G. Su, C.W. Chang, H.P. Wang, Y.C. Lin, W.C. Ou-Yang, I.W. Sun, *Int. J. Mol. Sci.,* 11 (2010) 329.
38. S.Y. Ku, S.Y. Lu, *Int. J. Electrochem. Sci.,* 6 (2011) 5219.
39. T.Y. Wu, M.H. Tsao, F.L. Chen, S.G. Su, C.W. Chang, H.P. Wang, Y.C. Lin, I.W. Sun, *J. Iran Chem. Soc.,* 7 (2010) 707.
40. M.H. Tsao, T.Y. Wu, H.P. Wang, I.W. Sun, S.G. Su, Y.C. Lin, C.W. Chang, *Mater. Lett.,* 65 (2011) 583.
41. T.Y. Wu, M.H. Tsao, S.G. Su, H.P. Wang, Y.C. Lin, F.L. Chen, C.W. Chang, I.W. Sun, *J. Braz. Chem. Soc.,* 22 (2011) 780.
42. M. Grätzel, *Nature*, 414 (2001) 338.
43. Q. Wang, J.-E. Moser, M. Grätzel, *J. Phys. Chem. B*, 109 (2005) 14945.
44. P. Wang, S.M. Zakeeruddin, P. Comte, R. Charvet, R. Humphry-Baker, M. Grätzel, *J. Phys. Chem. B*, 107 (2003) 14336.
45. E. Stathatos, P. Lianos, A. Surca Vuk, B. Orel, *Adv. Funct. Mater.,* 14 (2004) 45.
46. T.Y. Wu, B.K. Chen, C.W. Kuo, L. Hao, Y.C. Peng, I.W. Sun, *J. Taiwan Inst. Chem. Eng.,* (2012) http://dx.doi.org/10.1016/j.jtice.2012.06.001.
47. R. Kawano, H. Matsui, C. Matsuyama, A. Sato, M.A.B.H. Susan, N. Tanabe, M. Watanabe, *J. Photochem. Photobiol. A Chem.,* 164 (2004) 87.
48. T.Y. Wu, B.K. Chen, L. Hao, Y.C. Lin, H.P. Wang, C.W. Kuo, I.W. Sun, *Int. J. Mol. Sci.,* 12 (2011) 8750.
49. T.Y. Wu, S.G. Su, S.T. Gung, M.W. Lin, Y.C. Lin, W.C. Ou-Yang, I.W. Sun, C.A. Lai, *J. Iran. Chem. Soc.,* 8 (2011) 149.
50. T.Y. Wu, B.K. Chen, L. Hao, K.F. Lin, I.W. Sun, *J. Taiwan Inst. Chem. Eng.,* 42 (2011) 914.
51. T.Y. Wu, I.W. Sun, S.T. Gung, M.W. Lin, B.K. Chen, H.P. Wang, S.G. Su, *J. Taiwan Inst. Chem.*

Eng., 42 (2011) 513.
52. T.Y. Wu, H.C. Wang, S.G. Su, S.T. Gung, M.W. Lin, C.B. Lin, *J. Taiwan Inst. Chem. Eng.*, 41 (2010) 315.
53. T.Y. Wu, H.C. Wang, S.G. Su, S.T. Gung, M.W. Lin, C.B. Lin, *J. Chin. Chem. Soc.*, 57 (2010) 44.
54. T.Y. Wu, S.G. Su, Y.C. Lin, H.P. Wang, M.W. Lin, S.T. Gung, I.W. Sun, *Electrochim. Acta*, 56 (2010) 853.
55. I.W. Sun, Y.C. Lin, B.K. Chen, C.W. Kuo, C.C. Chen, S.G. Su, P.R. Chen, T.Y. Wu, *Int. J. Electrochem. Sci.*, 7 (2012) 7206.
56. T.Y. Wu, S.G. Su, H.P. Wang, I.W. Sun, *Electrochem. Commun.*, 13 (2011) 237.
57. T.Y. Wu, L. Hao, C.W. Kuo, Y.C. Lin, S.G. Su, P.L. Kuo, I.W. Sun, *Int. J. Electrochem. Sci.*, 7 (2012) 2047.
58. S.R. Starkey, R. Frech, *Electrochim. Acta*, 42 (1997) 471.
59. T. Asano, T. Kubo, Y. Nishikitani, *J. Photochem. Photobiol. A*, 164 (2004) 111.
60. M. Grätzel, *J. Photochem. Photobiol. A*, 164 (2004) 3.
61. M. Zistler, P. Wachter, P. Wasercheid, D. Gerhard, A. Hinsch, R. Sastrawan, H.J. Gores, *Electrochim. Acta*, 52 (2006) 161.
62. G. Boschloo, A. Hagfeldt, *J. Phys. Chem. B*, 109 (2005) 12093.
63. R. Komiya, L. Han, R. Yamanaka, A. Islam, T. Mitate, *J. Photochem. Photobiol. A*, 164 (2004) 123.